Optics Communications 305 (2013) 76–81

Contents lists available at SciVerse ScienceDirect

Optics Communications

journal homepage: www.elsevier.com/locate/optcom

Vortex strings in electric dipole radiation near a mirror

Xin Li [a,1], Henk F. Arnoldus [b,*]

[a] Department of Physics, Millersville University, P.O. Box 1002, Millersville, PA 17551, USA
[b] Department of Physics and Astronomy, Mississippi State University, P.O. Drawer 5167, Mississippi State, MS 39762-5167, USA

ARTICLE INFO

Article history:
Received 29 January 2013
Received in revised form
3 April 2013
Accepted 26 April 2013
Available online 18 May 2013

Keywords:
Optical vortex
Interference
Dipole radiation

ABSTRACT

The energy flow pattern of the radiation emitted by an oscillating electric dipole near a mirror has a complicated structure, including numerous singularities and vortices. We consider the flow lines of energy in the plane through the surface normal and the oscillation direction of the dipole. It is shown that the vortices are due to the vanishing of the magnetic field at their centers. The locations of the vortices have the appearance of beads on strings, and there are four such strings. The rotation direction of the energy flow for each vortex on a given string is the same. There are two strings with clockwise rotation and two strings with counterclockwise rotation. Field lines of energy flow either start or end at the center of a vortex. For a given string, field lines end at each vortex or field lines start at each vortex. There are two strings on which field lines end at the centers of the vortices, and there are two strings on which field lines start inside the vortices.

© 2013 Elsevier B.V. All rights reserved.

1. Introduction

The first prediction of an optical vortex was made by Wolter in 1950 [1]. He considered the reflection of a finite width light beam by an interface, and he showed that close to the interface a vortex should appear. At the center of this vortex is a singularity, where the direction of energy flow becomes undefined, and near the vortex the electromagnetic energy swirls around the singularity. Shortly afterward, Braunbek and Laukien [2] considered a half-infinite conducting sheet (the Sommerfeld half-plane), illuminated by a monochromatic plane wave under normal incidence. They found numerically that an optical vortex in the field lines of energy flow should appear at the illuminated side of the half-plane, somewhere near the edge. Singularities and vortices are sub-wavelength phenomena. In macroscopic optics (with incoherent sources), light appears to propagate along straight lines, which are the optical rays. On a sub-wavelength scale, however, light does not necessarily travel along straight lines. Energy flows along the field lines of the Poynting vector, and these field lines are in general curves. When light diffracts around an edge or scatters off a nanoscale object, the field line pattern of energy flow can have a very intricate structure in the vicinity of the object.

Singular optics originally focused on wavefront dislocations [3,4]. The most interesting type of singularity is a singularity at the center of an optical vortex in the energy flow pattern, and these Poynting vector vortices have been studied extensively [5–10]. Vortices around singular points have been predicted in the field diffracted through a sub-wavelength slit in a screen [11,12], in interference patterns between three plane waves [13] and in the focal plane of a lens [14–17]. By far the most studied optical vortices are the vortices in the field of a Laguerre–Gaussian laser beam [18–21]. Also, optical vortices, loops and knots can be generated in the laboratory by means of interference of light beams [22], and the existence of vortices can be experimentally verified with interference techniques [23–26]. A vortex of a different nature appears when there is some sort of rotation in the source. When an atom decays spontaneously in a $\Delta m = \pm 1$ electronic transition, the induced dipole moment rotates. As a result, the light is emitted in a vortex structure [27–31], with the field lines winding around an axis which is perpendicular to the circle that is traced out by the rotating dipole moment. Radiation emitted by higher-order multipoles has a similar vortex structure [32]. Also, when a small particle is irradiated by a circularly polarized laser beam, it emits radiation in a vortex pattern, and this has been observed experimentally by a measurement in the far field [33].

2. Electric dipole near a mirror

We consider an electric dipole, located on the z axis, and a distance H above the xy plane. The region $z<0$ is a perfect conductor, so the xy plane is the surface of a mirror. The dipole oscillates harmonically with angular frequency ω, so the electric dipole moment is

$$\mathbf{d}(t) = d_0 \boldsymbol{\varepsilon} \cos(\omega t). \tag{1}$$

* Corresponding author. Tel.: +1 662 325 2919; fax: +1 662 325 8898.
E-mail addresses: Xin.Li@millersville.edu (X. Li), hfa1@msstate.edu (H.F. Arnoldus).
[1] Tel.: +1 717 872 3756.

0030-4018/$ - see front matter © 2013 Elsevier B.V. All rights reserved.
http://dx.doi.org/10.1016/j.optcom.2013.04.078

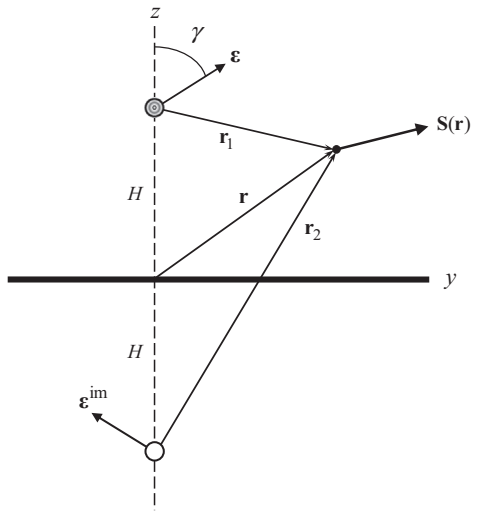

Fig. 1. The figure shows the setup of the electric dipole near a mirror, and the location and oscillation direction of the image dipole.

Here, d_o is the amplitude of the oscillation and $\boldsymbol{\varepsilon}$ is a unit vector. We take $\boldsymbol{\varepsilon}$ in the yz plane, and under an angle γ with the z axis, so that

$$\boldsymbol{\varepsilon} = \mathbf{e}_y \sin\gamma + \mathbf{e}_z \cos\gamma. \tag{2}$$

The setup is shown in Fig. 1. The oscillating dipole emits radiation, which is reflected by the surface of the mirror. The reflected field is identical to the field emitted by an image dipole, located on the z axis, and a distance H below the mirror. The dipole moment of the image dipole is [34]

$$\mathbf{d}(t)^{im} = d_o \boldsymbol{\varepsilon}^{im} \cos(\omega t), \tag{3}$$

with

$$\boldsymbol{\varepsilon}^{im} = -\mathbf{e}_y \sin\gamma + \mathbf{e}_z \cos\gamma. \tag{4}$$

3. Electric and magnetic fields

Since the dipole oscillates with angular frequency ω, so does the electric field and the magnetic field. The electric field can be written as

$$\mathbf{E}(\mathbf{r}, t) = \mathrm{Re}[\mathbf{E}(\mathbf{r}) e^{-i\omega t}], \tag{5}$$

with $\mathbf{E}(\mathbf{r})$ the complex amplitude. We then have

$$\mathbf{E}(\mathbf{r}) = \mathbf{E}(\mathbf{r})_s + \mathbf{E}(\mathbf{r})_r, \tag{6}$$

with $\mathbf{E}(\mathbf{r})_s$ the field emitted by the dipole (source), and $\mathbf{E}(\mathbf{r})_r$ the reflected field, which equals the field by the image dipole. Similar relations hold for the magnetic field $\mathbf{B}(\mathbf{r})$. Vector $\mathbf{r}$ represents the field point where we wish to compute the fields. It is convenient to introduce a vector $\mathbf{r}_1$, as shown in Fig. 1, which represents the same field point, but with respect to the location of the dipole. So we have

$$\mathbf{r}_1 = \mathbf{r} - H\mathbf{e}_z. \tag{7}$$

We shall use the wave number $k_o = \omega/c$ to go to dimensionless coordinates, so we set $\bar{x} = k_o x$, $\bar{y} = k_o y$ and $\bar{z} = k_o z$. On this scale, a distance of 2π corresponds to one optical wavelength. Similarly, we set $\mathbf{q}_1 = k_o \mathbf{r}_1$, and the magnitude of this vector is

$$q_1 = \sqrt{\bar{x}^2 + \bar{y}^2 + (\bar{z} - h)^2}, \tag{8}$$

with $h = k_o H$. The field point with respect to the image dipole is

$$\mathbf{r}_2 = \mathbf{r} + H\mathbf{e}_z, \tag{9}$$

and with $\mathbf{q}_2 = k_o \mathbf{r}_2$ we have

$$q_2 = \sqrt{\bar{x}^2 + \bar{y}^2 + (\bar{z} + h)^2}, \tag{10}$$

for the dimensionless distance between the image dipole and the field point.

The complex amplitudes of the electric and magnetic fields of an oscillating electric dipole are well known [35]. The complex amplitude of the electric field of the dipole is

$$\mathbf{E}(\mathbf{r})_s = \frac{d_o k_o^3}{4\pi\varepsilon_o q_1} \left\{ \boldsymbol{\varepsilon} - (\boldsymbol{\varepsilon}\cdot\hat{\mathbf{r}}_1)\hat{\mathbf{r}}_1 + \left[\boldsymbol{\varepsilon} - 3(\boldsymbol{\varepsilon}\cdot\hat{\mathbf{r}}_1)\hat{\mathbf{r}}_1\right] \frac{i}{q_1}\left(1 + \frac{i}{q_1}\right) \right\} e^{iq_1}, \tag{11}$$

with $\hat{\mathbf{r}}_1 = \mathbf{r}_1/r_1$ the unit vector from the dipole to the field point. This is the same as $\hat{\mathbf{r}}_1 = \mathbf{q}_1/q_1$. The magnetic field complex amplitude is

$$\mathbf{B}(\mathbf{r})_s = \frac{d_o k_o^3}{4\pi\varepsilon_o c q_1} (\hat{\mathbf{r}}_1 \cdot \boldsymbol{\varepsilon}) \left(1 + \frac{i}{q_1}\right) e^{iq_1}. \tag{12}$$

The complex amplitudes of the electric and magnetic fields of the image dipole are the same in form. We substitute $\boldsymbol{\varepsilon}^{im}$, q_2 and $\hat{\mathbf{r}}_2 = \mathbf{r}_2/r_2$ for $\boldsymbol{\varepsilon}$, q_1 and $\hat{\mathbf{r}}_1$, respectively, in Eqs. (11) and (12).

4. Poynting vector

At a field point $\mathbf{r}$, electromagnetic energy flows into the direction of the Poynting vector $\mathbf{S}$. For a time-harmonic field we consider the time-averaged Poynting vector, in which terms that oscillate at twice the optical frequency are discarded. These terms average to zero on a time scale of an optical cycle. This time-averaged Poynting vector is

$$\mathbf{S}(\mathbf{r}) = \frac{1}{2\mu_o} \mathrm{Re}\left[\mathbf{E}(\mathbf{r}) \times \mathbf{B}(\mathbf{r})^*\right]. \tag{13}$$

With the above expressions for the complex amplitudes of the electric and magnetic fields, this vector $\mathbf{S}(\mathbf{r})$ can be computed, but the result is cumbersome [36]. Electromagnetic radiation flows along the field lines of the vector field $\mathbf{S}(\mathbf{r})$. Let $\mathbf{r}(u)$ be a point on a field line, and here u is a variable which parametrizes the field line. Then a field line is the solution of

$$\frac{d\mathbf{r}}{du} = f(\mathbf{r})\mathbf{S}(\mathbf{r}), \tag{14}$$

with $f(\mathbf{r})$ a non-negative function of $\mathbf{r}$. We can choose this function arbitrarily, since field lines are determined by the direction of $\mathbf{S}(\mathbf{r})$, and not by its magnitude. This function can be chosen such as to optimize the step size in numerical integration. Eq. (14) determines the field line that goes through an initial point (x_o, y_o, z_o). The field lines in the figures in this paper are obtained by numerically solving Eq. (14). We use, of course, the dimensionless representation $\mathbf{q}(u) = k_o \mathbf{r}(u)$ for the figures.

5. Field lines in the *yz* plane

Vectors $\boldsymbol{\varepsilon}$ and $\boldsymbol{\varepsilon}^{im}$ are in the yz plane. When the field point $\mathbf{r}$ is in the yz plane, then so are $\hat{\mathbf{r}}_1$ and $\hat{\mathbf{r}}_2$, and therefore $\mathbf{E}(\mathbf{r})$ is in the yz plane, $\mathbf{B}(\mathbf{r})$ is along the x axis and the Poynting vector is in the yz plane. Consequently, a field line through a point in the yz plane lies entirely in the yz plane, whereas in general a field line is a three dimensional curve. We shall consider field lines in the yz plane. The field line pattern for $h = 2\pi$ and $\gamma = \pi/4$ is shown in Fig. 2. There appears to be a rich structure in the flow lines for the region shown in the figure. To the right of the dipole and above the dipole the field lines are more or less smooth, so these regions are not included in the figure. Two large vortices, labeled a and b, can be

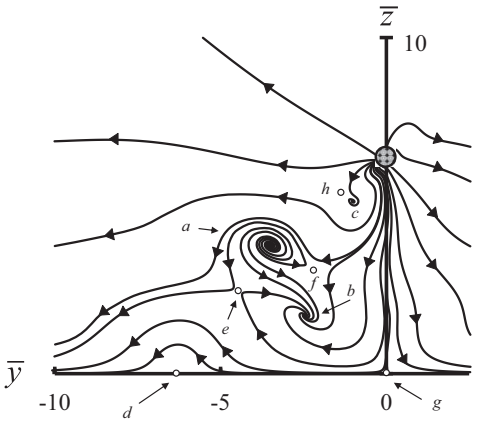

Fig. 2. The figure shows field lines of the Poynting vector for $h=2\pi$ and the dipole oscillating under 45° with the z axis ($\gamma=\pi/4$). There are many singularities and three vortices in this flow pattern.

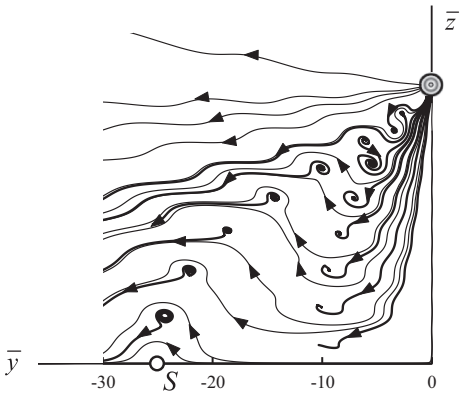

Fig. 3. Shown are field lines of the Poynting vector for $h=8\pi$ and $\gamma=\pi/4$. The bold field lines start or end at a vortex.

seen, and a very small vortex, labeled c, is present near the location of the dipole. Near vortex a, the field lines swirl around the singularity at its center in the counterclockwise direction, whereas for vortices b and c the rotation is clockwise. At vortex a, field lines come out of the center of the vortex, whereas at vortices b and c the field lines end at the centers of the vortices. Interestingly, some field lines start at the center of vortex a and end at the center of vortex b. Energy flowing along these field lines does not seem to originate from the location of the dipole, but it appears as if vortex a is the source of the energy. This is somewhat misleading, since the divergence of $\mathbf{S}$ is zero. The vector field $\mathbf{S}$ does not have a source other than the dipole, and it does not have sinks. The energy that seemingly comes out of the center of vortex a comes from field lines off the yz plane, running toward the vortex. Similarly, energy flowing along field lines that end at vortices b and c flows away off the yz plane.

Many singularities of a different type can be seen in the figure. For instance, near point e the field lines run into different directions and this can only happen in the neighborhood of a singular point. Singularity d is of particular interest, as we shall see below. In Fig. 2, it seems that the field lines jump over this point. It can be shown that this point is a point on a singular circle in the xy plane [36,37].

Fig. 3 shows the energy flow pattern for $h=8\pi$ and $\gamma=\pi/4$. The bold field lines start or end at a vortex. There appears to be a row of vortices on the left where all field lines rotate counterclockwise around the singularity at the center and the field lines start at the singularity. Fig. 4 shows an enlargement of one of these vortices. Below the vortex, field lines split, and therefore there must be a

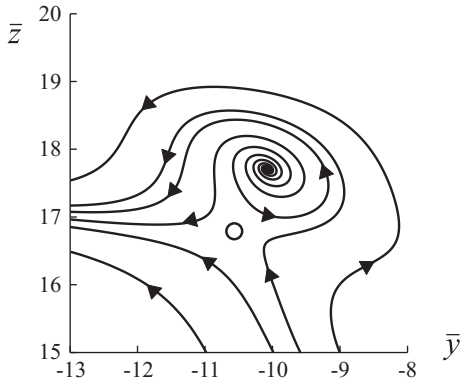

Fig. 4. The figure shows an enlargement of one of the vortices on the left in Fig. 3. The white circle is a singularity.

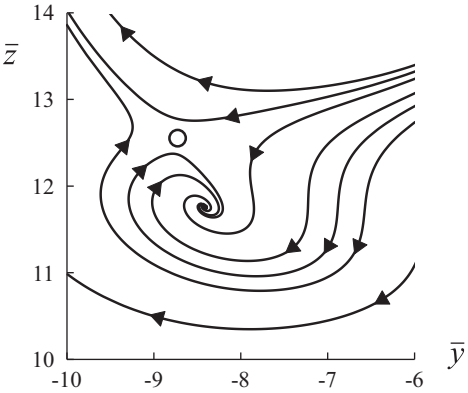

Fig. 5. The figure shows an enlargement of one of the vortices on the right in Fig. 3, and the white circle is a singularity.

singularity in this neighborhood. This point is indicated with a white circle. Near the vortices on the right, the field lines swirl around the singularity in a clockwise direction and the field lines end at the singularity. An enlargement of one of these vortices is shown in Fig. 5.

6. Location of the vortices

At a singularity, the Poynting vector vanishes. This can be either a result of $\mathbf{E}(\mathbf{r})=0$ or $\mathbf{B}(\mathbf{r})=0$ or $\mathbf{E}(\mathbf{r})\times\mathbf{B}(\mathbf{r})^*$ imaginary. At the vortices a, b and c in Fig. 2, and at point d, we have $\mathbf{B}(\mathbf{r})=0$, as we have determined numerically. At the other singularities we have $\mathbf{E}(\mathbf{r})\times\mathbf{B}(\mathbf{r})^*$ imaginary. The location of the vortices in Fig. 2 seems somewhat arbitrary, but in Fig. 3 a pattern seems to emerge. We now show that the vortices in Fig. 3 are a result of the magnetic field vanishing at the singularities at the centers of these vortices. The magnetic field at the field point $\mathbf{r}$ is

$$\mathbf{B}(\mathbf{r})=\frac{d_o k_o^3}{4\pi\varepsilon_o c}\left[\frac{e^{iq_1}}{q_1}\left(1+\frac{i}{q_1}\right)\hat{\mathbf{r}}_1\times\boldsymbol{\varepsilon}+\frac{e^{iq_2}}{q_2}\left(1+\frac{i}{q_2}\right)\hat{\mathbf{r}}_2\times\boldsymbol{\varepsilon}^{im}\right], \qquad (15)$$

with q_1 and q_2 given by Eqs. (8) and (10), respectively. Vectors $\boldsymbol{\varepsilon}$ and $\boldsymbol{\varepsilon}^{im}$ are given by Eqs. (2) and (4), respectively, and for a field point in the yz plane we have $\bar{x}=0$. The magnetic field only has an x component in the yz plane, and working out the right-hand side of Eq. (15) yields

$$B_x(\mathbf{r})=\frac{d_o k_o^3}{4\pi\varepsilon_o c}\left\{\frac{e^{iq_1}}{q_1^3}(q_1+i)\left[\bar{y}\cos\gamma+(h-\bar{z})\sin\gamma\right]\right.$$

$$+\frac{e^{iq_2}}{q_2^3}(q_2+i)\left[\bar{y}\cos\gamma+(h+\bar{z})\sin\gamma\right]\Bigg\} \tag{16}$$

Since the right-hand side of Eq. (16) is complex, the magnetic field vanishes when the real and the imaginary parts vanish simultaneously. For $\mathrm{Re}B_x(\mathbf{r})=0$ this gives

$$\frac{q_1\cos q_1-\sin q_1}{q_1^3}\left[\bar{y}\cos\gamma+(h-\bar{z})\sin\gamma\right]$$
$$+\frac{q_2\cos q_2-\sin q_2}{q_2^3}\left[\bar{y}\cos\gamma+(h+\bar{z})\sin\gamma\right]=0, \tag{17}$$

and for $\mathrm{Im}B_x(\mathbf{r})=0$ we have

$$\frac{q_1\sin q_1+\cos q_1}{q_1^3}\left[\bar{y}\cos\gamma+(h-\bar{z})\sin\gamma\right]$$
$$+\frac{q_2\sin q_2+\cos q_2}{q_2^3}\left[\bar{y}\cos\gamma+(h+\bar{z})\sin\gamma\right]=0. \tag{18}$$

Given h and γ, Eq. (17) defines a set of curves in the yz plane, and so does Eq. (18). At intersections of these curves, the magnetic field vanishes, and we have a singularity. The solid curves in Fig. 6 are the solutions of Eq. (17) and the dashed curves are the solutions of Eq. (18), and the parameters are the same as for Fig. 3. The intersections are highlighted with black dots, and we see indeed that these dots correspond to the locations of the vortices in Fig. 3. The two rows of vortices in Fig. 6 appear as beads on a string, and we shall call these the "vortex strings". The row on the left will be indicated as the A string and the row on the right as the B string.

Eqs. (17) and (18) are solved numerically. However, we can see one solution immediately

$$S:\ \bar{y}=-h\tan\gamma\ ,\ \ \bar{z}=0. \tag{19}$$

This is point S at the surface of the mirror in Figs. 3 and 6, and this is point d in Fig. 2. At this point, the magnetic field vanishes, but there is no vortex. We see from Fig. 6 that it is the endpoint of the A string. So, the A string runs from the dipole to point S, and the B string is in between the A string and the z axis. For a vertical dipole ($\gamma=0$), point S is at the origin of coordinates, and both strings coincide with the z axis. It follows from symmetry considerations that in this case there are no vortices on the z axis. Or, the spatial dimension of the vortices shrinks to zero in this limit. The location of point S has a simple geometrical construction, as shown in Fig. 7.

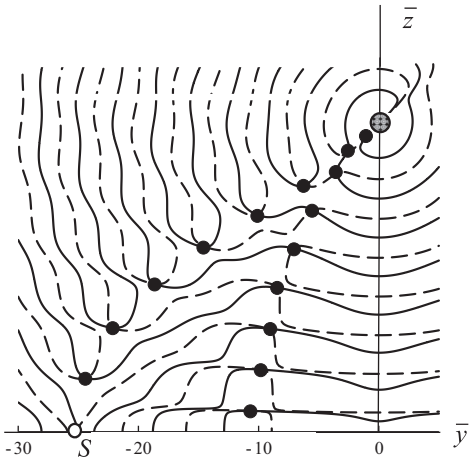

Fig. 6. The solid curves are the solutions of $\mathrm{Re}B_x(\mathbf{r})=0$ and the dashed curves are the solutions of $\mathrm{Im}B_x(\mathbf{r})=0$. The intersections are shown as black dots, and these points are the locations of vortices. The parameters for the figure are $h=8\pi$ and $\gamma=\pi/4$. Point S is located at $\bar{y}=-h\tan\gamma=-25.1$, and there are 15 vortices in the figure for these parameters.

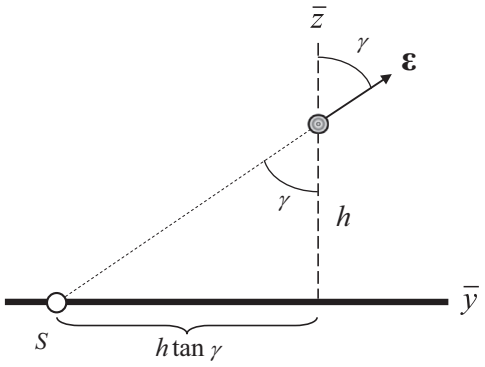

Fig. 7. The figure illustrates the construction to find point S on the surface of the mirror. The dipole oscillates along vector $\boldsymbol{\varepsilon}$. When we extend this line of oscillation, it intersects the mirror at point S.

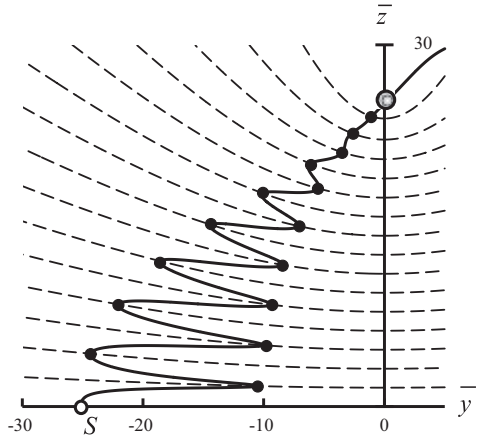

Fig. 8. The solid curve is the solution of Eq. (21) and the dashed curves are the solutions of Eq. (22), for $h=8\pi$ and $\gamma=\pi/4$. Vortices are located at the intersections, and these points are indicated by black dots.

7. Vortex strings

Vortices appear when $B_x(\mathbf{r})=0$, with $B_x(\mathbf{r})$ given by Eq. (16). Rather than considering the real and imaginary parts of this equation, we first multiply by $q_2^3(q_1-i)\exp(-iq_1)$. This gives

$$(q_1-i)(q_2+i)\left[\bar{y}\cos\gamma+(h+\bar{z})\sin\gamma\right]e^{i(q_2-q_1)}$$
$$+\left(\frac{q_2}{q_1}\right)^3(q_1^2+1)\left[\bar{y}\cos\gamma+(h-\bar{z})\sin\gamma\right]=0. \tag{20}$$

The left-hand side is complex. Setting the real and imaginary parts equal to zero gives

$$\left[(q_1q_2+1)\cos(q_2-q_1)+(q_2-q_1)\sin(q_2-q_1)\right]\left[\bar{y}\cos\gamma+(h+\bar{z})\sin\gamma\right]$$
$$+\left(\frac{q_2}{q_1}\right)^3(q_1^2+1)\left[\bar{y}\cos\gamma+(h-\bar{z})\sin\gamma\right]=0, \tag{21}$$

and

$$(q_1q_2+1)\sin(q_2-q_1)=(q_2-q_1)\cos(q_2-q_1), \tag{22}$$

respectively.

Eqs. (21) and (22) define two sets of curves, and the intersections indicate the locations of the vortices. There is a great advantage in using Eqs. (21) and (22) instead of Eqs. (17) and (18). The solid curve in Fig. 8 is the solution of Eq. (21) for $h=8\pi$ and $\gamma=\pi/4$, and the set of dashed curves are the solutions of Eq. (22). As compared to Fig. 6, for which we have the same parameters, it is now much more clear where the vortices appear. Eq. (22) is independent of the orientation γ of the dipole. So, when we vary γ, then the solid curve in Fig. 8

changes with it, but the dashed curves remain the same. At the location of the dipole, we have $\bar{y}=0$, $\bar{z}=h$, $q_1=0$ and $q_2=2h$. We see that this is a solution of Eq. (21), so the solid curve goes through the dipole. From Eq. (22) we see the solution $q_2=q_1$, and this is the y axis. When we set $q_2=q_1$ in Eq. (21), we find $\bar{y}=-h\tan\gamma$, and this is point S. Therefore, the solid curve in the figure runs from the dipole to point S on the mirror.

The intersections between the solid curve and the dashed curves in Fig. 8 are the locations of the vortices. The intersections at the left side of the solid curve form the A string, and a vortex on this string has the appearance as in Fig. 4. The intersections on the right lie on the B string, and a typical vortex is shown in Fig. 5. We notice from Fig. 8 that the solid curve runs through the dipole and continues into the region $\bar{z}>h$. Fig. 9 shows a larger view, and we see that far away from the dipole there are also intersections between the solid curve and the dashed curves. These intersections also correspond to vortices in the energy flow pattern, and we shall call this series of vortices the C string. For vortices on the C string, field lines end at the vortex, and the field lines wind around the singular point in the counterclockwise direction.

Fig. 10 shows the location of the vortices for $h=4\pi$ and $\gamma=60^\circ$. Point S is located at $\bar{y}=-h\tan\gamma=-21.7$. Here, γ is larger than in Fig. 9, and we see that the vortices on the C string come closer to the location of the dipole. There are three vortices on the A string, four on the B string, and four on the C string. Fig. 11 shows the energy flow pattern for the same parameters as in Fig. 10.

When we increase γ, with h fixed, point S moves to the left, and for $\gamma\to 90^\circ$ this point drifts off to infinity. For $\gamma=90^\circ$, the figure should be symmetric between left and right, so then the C string is the reflection in the z axis of the B string. Fig. 12 shows the vortex strings for $\gamma=90^\circ$ and $h=30\pi$. We notice that, although point S moves to infinity, the A string is still present. Its reflection in the z axis is a series of vortices on the right, and we shall call this the D string. Near these vortices, the field lines rotate clockwise, and they start at the singularity at the center. For smaller values of h, the B and the C strings come relatively closer to the z axis, and vortices on the A and the D strings move further away from the dipole.

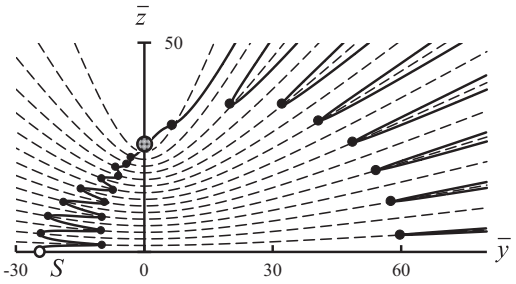

Fig. 9. The figure shows a larger view of the picture in Fig. 8. We see that the solid curve intersects the dashed curves at large distances from the dipole. The corresponding vortices form the C string.

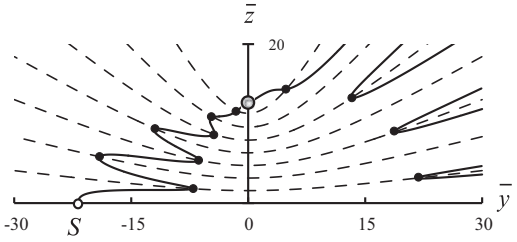

Fig. 10. For this figure we have $h=4\pi$ and $\gamma=\pi/3$. We see that the vortices to the right of the z axis are closer to the dipole than in Fig. 9, which is due to the fact that γ is larger.

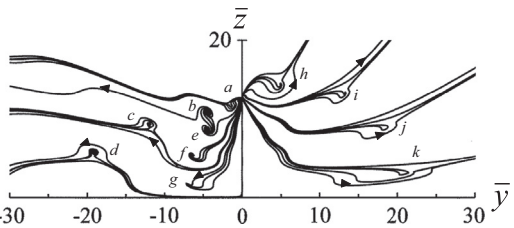

Fig. 11. The figure shows the field line pattern of energy flow for $h=4\pi$ and $\gamma=\pi/3$, and these parameters are the same as for Fig. 10. Vortices b, c and d lie on the A string and vortices e, f and g are on the B string. Vortex a is very close to the dipole, and we see from Fig. 10 that we should assign this vortex to the B string. The vortices h, i, j and k on the right are on the C string.

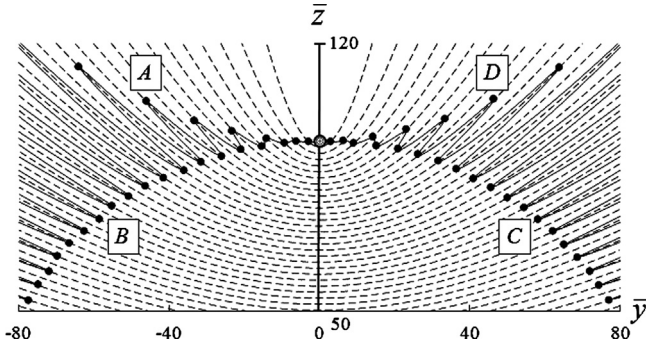

Fig. 12. The figure shows the location of the vortices for $\gamma=\pi/2$ and $h=30\pi$. There are four vortex strings, labeled A, B, C and D.

The vortices in the energy flow of radiation emitted by an electric dipole near a mirror lie on four strings. When the dipole oscillates parallel to the mirror surface ($\gamma=90^\circ$), we have the situation as shown in Fig. 12. The flow pattern is reflection symmetric with respect to the z axis, and there are two strings at each side of the z axis. For smaller γ, the A string moves down, and ends at point S on the mirror surface. Since the B string is in between the A string and the z axis, this string moves closer to the z axis. The C and the D strings move upward, and the D string moves out of the picture quickly, as can be seen in Figs. 9 and 10. For even smaller γ, the vortices on the C string are far away from the dipole, and move out of the picture. Then only the vortices on the A and B strings remain near the dipole, and the situation is as in Fig. 8. For $\gamma\to 0$, point S moves to $\bar{y}=0$, and both the A and the B strings coincide with the z axis below the dipole.

8. Distance between vortices on a string

Fig. 12 shows that the vortices along the B and the C strings are approximately equally spaced. From Fig. 8 we observe that the vortices along the A string are spaced by about the same distance as the vortices along the B string for the value of γ used for the figure. When a string extends to the region above the dipole, as for A and D in Fig. 12, and for C in Fig. 9, the separation between the vortices along a string is considerably larger. We shall consider the separation of vortices along a string in the region below the dipole, and make an approximation for this distance. Vortices are located on the intersections of the solid and dashed curves in the figures. When we follow a solid curve, as for instance in Fig. 8, the vortices along the solid curve alternate between the A and the B strings. The dashed curves are more or less equally spaced, and therefore the distance between vortices along a string is about twice the separation of the dashed curves. To find the separation between the dashed curves, we consider their intersections with the $\bar{z}$ axis. The dashed curves are the solutions of Eq. (22), with q_1 and q_2

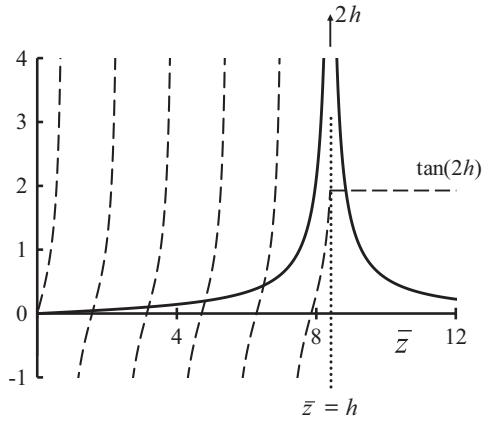

Fig. 13. The intersections between the solid curve and the dashed curves correspond to a solution of Eq. (22) on the $\bar{z}$ axis.

given by Eqs. (8) and (10), respectively. In the $\bar{y}\bar{z}$ plane we have $\bar{x}=0$, and on the $\bar{z}$ axis we have $\bar{y}=0$. So we have

$$q_1 = \begin{cases} h-\bar{z} & , \quad 0\le\bar{z}\le h \\ \bar{z}-h & , \quad \bar{z}\ge h \end{cases}, \tag{23}$$

$$q_2 = \bar{z}+h \tag{24}$$

Eq. (22) becomes

$$\frac{2\bar{z}}{1+h^2-\bar{z}^2} = \tan(2\bar{z}), \quad 0\le\bar{z}\le h, \tag{25}$$

$$\frac{2h}{1-h^2+\bar{z}^2} = \tan(2h), \quad \bar{z}\ge h. \tag{26}$$

The left-hand sides of Eqs. (25) and (26) are the solid curves in Fig. 13, and the right-hand sides are the dashed curves. At a value of $\bar{z}$ where the curves intersect, we have a solution of Eq. (22). The solid curve in Fig. 13 is continuous at $\bar{z}=h$, and the height of the peak is $2h$. For $\bar{z}<h$, the intersections are approximately the zeros of $\tan(2\bar{z})$, and these are $\pi/2$ apart. Therefore, the vortices on a string are about π apart. In dimensionless coordinates, 2π corresponds to an optical wavelength, and so the vortices along a string are about half a wavelength apart. We also see from the figure that for $\bar{z}>h$ there is at most one solution. This is consistent with Figs. 8–10 and 12, where we see that there are no dashed curves intersecting the $\bar{z}$ axis for $\bar{z}>h$.

9. Conclusions

When an oscillating electric dipole is located near the surface of a mirror, the emitted radiation interferes with the radiation reflected by the surface. This results in the appearance of numerous singularities and vortices in the energy flow pattern, as can be seen from Fig. 2. The problem has only two free parameters: the dimensionless distance h between the dipole and the mirror surface, and the angle between the surface normal and the oscillation direction of the dipole (γ). We consider flow lines of energy in the plane through the surface normal and the oscillation direction of the dipole, as illustrated in Fig. 1.

At the center of a vortex is a singularity, and it is shown that these singularities are due to the vanishing magnetic field at these points. Despite the complicated flow pattern of energy, it was found that the location of the vortices in the flow pattern has a very simple structure. Vortices appear as beads on strings, and there are four such strings, as is most easily seen from Fig. 12. The string named A runs from the dipole to point S on the surface, with the coordinates of S given by Eq. (19). String B is in between string A and the z axis. String C runs from the dipole to the surface of the mirror, but it is much further away from the z axis than the B string. A fourth string, D, starts at the dipole and runs away to the upper right in the figures. Vortices on this string are very far away from the dipole, and cannot be seen in the figures, except in Fig. 12. The vortices along a string are separated by about half a wavelength, except for the vortices that are far away from the dipole.

The direction of rotation in the energy flow near a vortex can be counterclockwise, as in Fig. 4, or clockwise, as in Fig. 5. And, the circulating energy near a vortex can come out of the vortex, as in Fig. 4, or end in the vortex, as in Fig. 5. It was found that the direction of rotation in vortices on the A and the C strings is counterclockwise, and for the B and the D strings the rotation is clockwise. On the A and the D string, the energy comes out of the vortex, and on the B and the C string the energy ends in the vortex.

References

[1] H. Wolter, Zeitschrift für Naturforschung 5a (1950) 278. (translated in: H. Wolter, Journal of Optics A: Pure and Applied Optics 11 (2009) 090401 (7 pp.)).
[2] W. Braunbek, G. Laukien, Optik 9 (1952) 174.
[3] J.F. Nye, M.V. Berry, Proceedings of the Royal Society of London A 336 (1974) 165.
[4] M.S. Soskin, M.V. Vasnetsov, Progress in Optics 42 (2001) 219.
[5] M.V. Berry, Journal of Physics A: Mathematical and General 38 (2005) L745.
[6] I. Mokhun, R. Brandel, Ju. Viktorovskaya, Ukrainian Journal of Physical Optics 7 (2006) 63.
[7] I. Mokhun, A. Mokhun, Ju. Viktorovskaya, Ukrainian Journal of Physical Optics 7 (2006) 129.
[8] I. Mokhun, R. Khrobatin, Journal of Optics A: Pure and Applied Optics 10 (2008) 064015 (10 pp.).
[9] M.V. Berry, Journal of Optics A: Pure and Applied Optics 11 (2009) 094001 (12 pp.).
[10] I. Mokhun, A. Arkhelyuk, Y. Galushko, Y. Kharitonovtta, Ju. Viktorovskaya, Applied Optics 51 (2012) C158.
[11] H.F. Schouten, T.D. Visser, G. Gbur, D. Lenstra, H. Blok, Optics Express 11 (2003) 371.
[12] H.F. Schouten, T.D. Visser, D. Lenstra, H. Blok, Physical Review E 67 (2003) 036608-1.
[13] J. Masajada, B. Dubik, Optics Communications 198 (2001) 21.
[14] B. Richards, E. Wolf, Proceedings of the Royal Society of London 253 (1959) 358.
[15] A. Boivin, J. Dow, E. Wolf, Journal of the Optical Society of America 57 (1967) 1171.
[16] G.P. Karman, M.W. Beijersbergen, A. van Duijl, J.P. Woerdman, Optics Letters 22 (1997) 1503.
[17] J.T. Foley, E. Wolf, Optics Letters 30 (2005) 1312.
[18] M. Vasnetsov, K. Staliunas (Eds.), Optical Vortices, Horizons in World Physics, 228, Nova Science, Commack, New York, 1999.
[19] A.V. Volyar, V.G. Shvedov, T.A. Fadeeva, Optics and Spectroscopy 90 (2001) 93.
[20] V.A. Pas'co, M.S. Soskin, M.V. Vasnetsov, Optics Communications 198 (2001) 49.
[21] A.V. Volyar, T.A. Fadeeva, V.G. Shvedov, Optics and Spectroscopy 93 (2002) 267.
[22] J. Leach, M.R. Dennis, J. Courtial, M.J. Padgett, New Journal of Physics 7 (2005) 55.
[23] G. Molina-Terriza, L. Torner, D.V. Petrov, Optics Letters 24 (1999) 899.
[24] I. Freund, Optics Letters 26 (2001) 1996.
[25] I. Freund, A.I. Mokhun, M.S. Soskin, O.V. Angelsky, I.I. Mokhun, Optics Letters 27 (2002) 545.
[26] V.G. Denisenko, A. Minovich, A.S. Desyatnikov, W. Krolikowski, M.S. Soskin, Y.S. Kivshar, Optics Letters 33 (2008) 89.
[27] W. Gough, European Journal of Physics 7 (1986) 81.
[28] H.F. Arnoldus, J.T. Foley, Optics Communications 231 (2004) 115.
[29] H.F. Arnoldus, X. Li, J. Shu, Optics Letters 33 (2008) 1446.
[30] J. Shu, X. Li, H.F. Arnoldus, Journal of Modern Optics 55 (2008) 2457.
[31] J. Shu, X. Li, H.F. Arnoldus, Journal of the Optical Society of America A 26 (2009) 395.
[32] H.F. Arnoldus, Optics Communications 252 (2005) 253.
[33] D. Haefner, S. Sukhov, A. Dogariu, Physical Review Letters 102 (2009) 123903-1.
[34] H.F. Arnoldus, Journal of Modern Optics 54 (2007) 45.
[35] J.D. Jackson, Classical Electrodynamics, 3rd ed., Wiley, New York, 411.
[36] X. Li, H.F. Arnoldus, Physical Review A 81 (2010) 053844-1.
[37] X. Li, J. Shu, H.F. Arnoldus, Optics Letters 34 (2009) 3595.